

PCCP

Accepted Manuscript



This is an *Accepted Manuscript*, which has been through the Royal Society of Chemistry peer review process and has been accepted for publication.

Accepted Manuscripts are published online shortly after acceptance, before technical editing, formatting and proof reading. Using this free service, authors can make their results available to the community, in citable form, before we publish the edited article. We will replace this *Accepted Manuscript* with the edited and formatted *Advance Article* as soon as it is available.

You can find more information about *Accepted Manuscripts* in the [Information for Authors](#).

Please note that technical editing may introduce minor changes to the text and/or graphics, which may alter content. The journal's standard [Terms & Conditions](#) and the [Ethical guidelines](#) still apply. In no event shall the Royal Society of Chemistry be held responsible for any errors or omissions in this *Accepted Manuscript* or any consequences arising from the use of any information it contains.

Computational Study of the Rayleigh Light Scattering Properties of Atmospheric Pre-Nucleation Clusters†

Jonas Elm,^{*a} Patrick Norman,^b Merete Bilde,^c and Kurt V. Mikkelsen^a

Received Xth XXXXXXXXXXXX 20XX, Accepted Xth XXXXXXXXXXXX 20XX

First published on the web Xth XXXXXXXXXXXX 200X

DOI: 10.1039/b000000x

The Rayleigh and hyper Rayleigh scattering properties of the binary $(\text{H}_2\text{SO}_4)(\text{H}_2\text{O})_n$ and ternary $(\text{H}_2\text{SO}_4)(\text{NH}_3)(\text{H}_2\text{O})_n$ clusters are investigated using a quantum mechanical response theory approach. The molecular Rayleigh scattering intensities are expressed from the dipole polarizability α and hyperpolarizability β tensors. Using density functional theory, we elucidate the effect of cluster morphology on the scattering properties from a combinatorial sampling approach. We find that the Rayleigh scattering intensity depends quadratically on the number of water molecules in the cluster and that a single ammonia molecule is able to induce a high anisotropy, which further increases the scattering intensity. The hyper Rayleigh scattering activities are found to be extremely low. This study presents a first attempt to map the scattering of atmospheric molecular clusters using a bottom-up approach.

1 - Introduction

Atmospheric aerosols are unambiguously regarded as the largest uncertainty regarding climate estimation. Through the *indirect effect*, aerosols can affect the formation and properties of clouds¹. Via the *direct effect*, aerosols influence the climate either by acting as scatterers or absorbers of incident solar radiation². Aerosol particles are emitted directly into the atmosphere from various sources including combustion processes and wave breaking³. They are also formed in the atmosphere via nucleation and growth⁴. The exact mechanism of nucleation remains unclear, but is believed to occur through formation of $\text{H}_2\text{SO}_4\text{-H}_2\text{O-X}$ clusters. Suggestions for the nature of the stabilizer molecule X includes ammonia⁵⁻⁹, amines¹⁰⁻¹⁶, oxidized organics^{4,17-37} or ions³⁸⁻⁴⁶. The light scattering properties of molecules, clusters and particles in the atmosphere is determined by their size and the wavelength of the incoming light. The scattering of light by particles with the same size as the wavelength of the incoming light is described by Mie theory⁴⁷. For individual molecules, clusters and particles with diameter much lower than the wave length of the incoming radiation Rayleigh scattering is the dominant

mechanism⁴⁸⁻⁵¹.

It has recently become evident that the atmosphere contains a large pool of neutral molecular clusters⁵²⁻⁵⁵ with sizes below 2 nm. While some of these clusters grow to larger sizes and nucleate, a large fraction remain in the cluster pool. Concentrations reported are in the range $100\text{-}100.000\text{ cm}^{-3}$ ⁵³⁻⁵⁵. Understanding of the climate impact of this pool of clusters is lacking. The focus of this work is therefore the optical properties of atmospheric pre-nucleation clusters. For these clusters Rayleigh scattering is the dominant scattering mechanism.

The average size of clusters formed in molecular beams has previously been probed via Rayleigh scattering⁵⁶. Rayleigh scattering has also been used to analyse hydrogen-bonded systems by means of ab initio calculations⁵⁷⁻⁶⁰ as well as to analyse the difference in α -helix and β -sheets⁶¹ in proteins. To our knowledge this is however the first study targeted at elucidating the Rayleigh scattering properties of a series of clusters of relevance for the pool of pre-nucleation clusters in the atmosphere of Earth.

In a bottom-up approach we use quantum mechanical response theory to investigate cluster optical properties. This approach is not limited to spherical particles. As model systems we study pre-nucleation molecular clusters consisting of H_2O , NH_3 and H_2SO_4 molecules.

2 - Theory

2.1 - Polarizabilities and Scattering Intensities

The charge distribution of a chemical system will be influenced by an external electric field leading to polarization.

† Electronic Supplementary Information (ESI) available: All identified lowest Gibb's free energy minimum structures and polarizabilities for the $(\text{H}_2\text{SO}_4)(\text{H}_2\text{O})_n$ and $(\text{H}_2\text{SO}_4)(\text{NH}_3)(\text{H}_2\text{O})_n$ clusters for n up to 10 are available as supporting information. See DOI: 10.1039/b000000x/

^aDepartment of Chemistry, H. C. Ørsted Institute, University of Copenhagen, Universitetsparken 5, DK-2100 Copenhagen, Denmark E-mail: elm@chem.ku.dk

^bDepartment of Physics, Chemistry and Biology, Linköping University, SE-581 83 Linköping, Sweden

^cDepartment of Chemistry, Aarhus University, Langelandsgade 140, DK-8000 Århus C, Denmark

The field dependent induced dipole moment $\mu_i(\mathcal{E})$ can be expanded in a Taylor series in the electric field:

$$\mu_i(\mathcal{E}) = \mu_i^0 + \sum_j \alpha_{ij} \mathcal{E}_j + \frac{1}{2} \sum_{jk} \beta_{ijk} \mathcal{E}_j \mathcal{E}_k + \frac{1}{6} \sum_{jkl} \gamma_{ijkl} \mathcal{E}_j \mathcal{E}_k \mathcal{E}_l \dots \quad (1)$$

Here α_{ij} , β_{ijk} and γ_{ijkl} are the dipole polarizability, first hyperpolarizability and second hyperpolarizability, respectively. These quantities are represented by second-, third- and fourth-rank tensors with the Cartesian components ij , ijk and $ijkl$. Due to the dependence on the electric field, the polarizabilities are referred to as linear, quadratic and cubic responses to the electric field. For randomly oriented molecules in the gas phase, isotropic variants can be defined. For the polarizability α_{ij} the isotropic mean ($\bar{\alpha}$) and anisotropic ($\Delta\alpha$) polarizabilities are defined as:

$$\bar{\alpha} = \frac{1}{3} \sum_i \alpha_{ii} \quad (2)$$

$$\Delta\alpha = \sqrt{\frac{\sum_{ij} (3\alpha_{ij}\alpha_{ij} - \alpha_{ii}\alpha_{jj})}{2}} \quad (3)$$

Similarly two isotropic averages $\langle\beta_{ZZZ}^2\rangle$ and $\langle\beta_{XZZ}^2\rangle$ can be defined for the first hyperpolarizability⁶². The Rayleigh scattering activities of the $\mathfrak{R}_{p\parallel}$, $\mathfrak{R}_{p\perp}$ components of the linearly polarized light and \mathfrak{R}_n of natural light are given by:

$$\mathfrak{R}_n = 45(\bar{\alpha})^2 + 13(\Delta\alpha)^2 \quad (4)$$

$$\mathfrak{R}_{p\perp} = 45(\bar{\alpha})^2 + 7(\Delta\alpha)^2 \quad (5)$$

$$\mathfrak{R}_{p\parallel} = 6(\Delta\alpha)^2 \quad (6)$$

Hyper Rayleigh scattering corresponds to the elastic scattering of two incident photons into one with twice the frequency. The hyper Rayleigh scattering intensity of a plane polarized incident light wave and observation made perpendicular to the propagation is given by:

$$\mathfrak{R}_{\text{HRS}} = \sqrt{\langle\beta_{ZZZ}^2\rangle + \langle\beta_{XZZ}^2\rangle} \quad (7)$$

The so-called depolarization ratio (ρ) is an important parameter in measurements of scattered light. It is defined as the ratio between the parallel and perpendicular intensities to the scattering plane. For Rayleigh scattering, the depolarization ratio of natural light ρ_n , plane-polarized light ρ_p and circularly polarized light ρ_c are given by:

$$\rho_n = \frac{6(\Delta\alpha)^2}{45(\bar{\alpha})^2 + 7(\Delta\alpha)^2} \quad (8)$$

$$\rho_p = \frac{3(\Delta\alpha)^2}{45(\bar{\alpha})^2 + 4(\Delta\alpha)^2} \quad (9)$$

$$\rho_c = \frac{\rho_n}{1 - \rho_n} \quad (10)$$

The largest depolarization ratio corresponds to the most anisotropic case. Due to the non-zero value of $\bar{\alpha}$ the maximum value of ρ_n is $\frac{1}{2}$, while the maximum value of ρ_p is $\frac{1}{3}$. For ρ_c the maximum obtainable value is 1. Analogously, the hyper-Rayleigh depolarization ratio (ρ_{HRS}) which depends on the first hyperpolarizability can be defined as the ratio between the isotropic $\langle\beta_{ZZZ}^2\rangle$ and $\langle\beta_{XZZ}^2\rangle$ components:

$$\rho_{\text{HRS}} = \frac{\langle\beta_{ZZZ}^2\rangle}{\langle\beta_{XZZ}^2\rangle} \quad (11)$$

The hyper Rayleigh depolarization ratio can take values from ~ 1.5 in octopolar molecules to ~ 5.0 in pure dipolar molecules. From these equations, it is possible to evaluate the Rayleigh and hyper Rayleigh scattering intensities and polarization ratios of atmospheric pre-nucleation clusters. For analyzing the scattering properties, the binding mean isotropic and anisotropic polarizabilities are defined as the following:

$$\bar{\alpha}_{\text{Binding}} = \bar{\alpha}_{\text{Cluster}} - \sum_i \bar{\alpha}_{\text{Monomer},i} \quad (12)$$

$$\Delta\alpha_{\text{Binding}} = \Delta\alpha_{\text{Cluster}} - \sum_i \Delta\alpha_{\text{Monomer},i} \quad (13)$$

2.2 - Response Theory

The frequency dependent polarizability and hyperpolarizability can be calculated from linear and quadratic response theory methods. The linear response function is given by⁶³:

$$\langle\langle\hat{A}; \hat{V}^\omega\rangle\rangle_\omega = \sum_{n \neq 0} \left[\frac{\langle 0|\hat{A}|n\rangle\langle n|\hat{V}^\omega|0\rangle}{\omega_{n0} - \omega} + \frac{\langle 0|\hat{V}^\omega|n\rangle\langle n|\hat{A}|0\rangle}{\omega_{n0} + \omega} \right]$$

Here \hat{A} is our observable of interest and \hat{V}^ω is the perturbation operator. From the linear response function the property of interest can be obtained. In the case of the frequency dependent polarizability: $\alpha_{\alpha\beta}(-\omega; \omega) = -\langle\langle\mu_\alpha; \mu_\beta\rangle\rangle_\omega$. Similarly, the quadratic response function is given by:

$$\begin{aligned} \langle\langle\hat{A}; \hat{V}^{\omega_1}, \hat{V}^{\omega_2}\rangle\rangle_{\omega_1, \omega_2} = \sum_{k, n \neq 0} \left[\right. & \frac{\langle 0|\hat{A}|k\rangle\langle k|\hat{V}^{\omega_1} - \langle 0|\hat{V}^{\omega_1}|0\rangle|n\rangle\langle n|\hat{V}^{\omega_2}|0\rangle}{(\omega_1 + \omega_2 - \omega_k)(\omega_2 - \omega_n)} \\ & + \frac{\langle 0|\hat{V}^{\omega_2}|n\rangle\langle n|\hat{V}^{\omega_1} - \langle 0|\hat{V}^{\omega_1}|0\rangle|k\rangle\langle k|\hat{A}|0\rangle}{(\omega_1 + \omega_2 + \omega_k)(\omega_2 + \omega_n)} \\ & - \frac{\langle 0|\hat{V}^{\omega_1}|k\rangle\langle k|\hat{A} - \langle 0|\hat{A}|0\rangle|n\rangle\langle n|\hat{V}^{\omega_2}|0\rangle}{(\omega_1 + \omega_k)(\omega_2 - \omega_n)} \\ & + \frac{\langle 0|\hat{A}|k\rangle\langle k|\hat{V}^{\omega_2} - \langle 0|\hat{V}^{\omega_2}|0\rangle|n\rangle\langle n|\hat{V}^{\omega_1}|0\rangle}{(\omega_1 + \omega_2 - \omega_k)(\omega_1 - \omega_n)} \\ & - \frac{\langle 0|\hat{V}^{\omega_1}|n\rangle\langle n|\hat{V}^{\omega_2} - \langle 0|\hat{V}^{\omega_2}|0\rangle|k\rangle\langle k|\hat{A}|0\rangle}{(\omega_1 + \omega_2 + \omega_k)(\omega_1 - \omega_n)} \\ & \left. + \frac{\langle 0|\hat{V}^{\omega_2}|n\rangle\langle n|\hat{A} - \langle 0|\hat{A}|0\rangle|n\rangle\langle n|\hat{V}^{\omega_1}|0\rangle}{(\omega_2 + \omega_k)(\omega_1 - \omega_n)} \right] \end{aligned}$$

The quadratic response function can be used to gain insight into two-photon absorption transitions with the corresponding first hyper polarizability as the residue: $\beta_{\alpha\beta\gamma}(-\omega_\sigma; \omega_1, \omega_2) = \langle\langle\mu_\alpha; \mu_\beta, \mu_\gamma\rangle\rangle_{\omega_1, \omega_2}$.

3 - Computational Methodology

3.1 - Cluster Sampling

All calculations have been performed using the Gaussian09 program package⁶⁴. On the basis of recent benchmarks^{65–68}, the M06-2X⁶⁹ functional was chosen for calculating the molecular geometries and harmonic frequencies of the pre-nucleation clusters.

Two types of clusters consisting of H_2SO_4 , NH_3 and H_2O are investigated: The binary $(\text{H}_2\text{SO}_4)(\text{H}_2\text{O})_n$ and ternary $(\text{H}_2\text{SO}_4)(\text{NH}_3)(\text{H}_2\text{O})_n$ systems. We wish to investigate the dependence of the optical properties on cluster morphology and use a combinatorial approach to sample the structures. This is performed by defining a rigid cluster core (H_2SO_4 or $(\text{H}_2\text{SO}_4)(\text{NH}_3)$) and add the H_2O molecules at different sites around the cluster core. Using this approach results in two indistinguishable sites around a rigid C_2 -symmetric H_2SO_4 cluster core and two distinguishable sites around the C_1 -symmetric $(\text{H}_2\text{SO}_4)(\text{NH}_3)$ core.

The different cluster conformations will be denoted as [Site 1 - Site 2], where clusters with ammonia always will have ammonia attached to Site 2. For instance a cluster containing $(\text{H}_2\text{SO}_4)(\text{H}_2\text{O})_3$ would imply two combinations: a [0-3] combination with all water at one site and a [1-2] combination with one water at one site and two water at the other, as demonstrated in Figure 1. A $(\text{H}_2\text{SO}_4)(\text{NH}_3)(\text{H}_2\text{O})_3$ cluster would imply four combinations ([0-3], [1-2], [2-1] and [3-0]), since the core is no longer C_2 -symmetric due to the attached ammonia molecule, as seen in Figure 1.

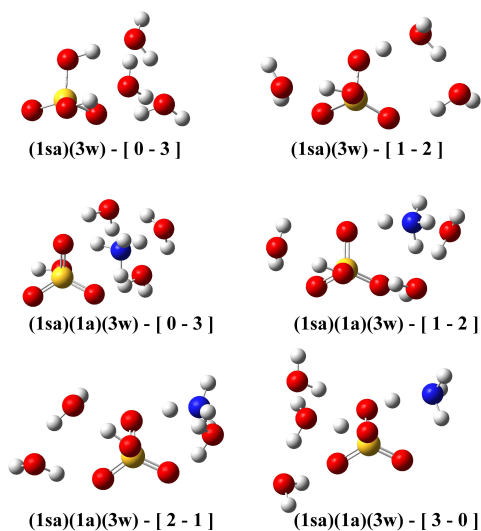


Fig. 1 Examples of the combinatorial sampled structures for $(\text{H}_2\text{SO}_4)(\text{H}_2\text{O})_3$ and $(\text{H}_2\text{SO}_4)(\text{NH}_3)(\text{H}_2\text{O})_3$ clusters.

Each combinatorial conformation is initially sampled using a Born Oppenheimer molecular dynamics (BOMD) approach using simulated annealing with the M06-2X/6-31+G(d,p) level of theory. In the molecular dynamics simulation the system is heated by an initial energy of ~ 5 kcal/mol for each water molecule which is uniformly removed over a time period of up to 5 ps. In all cases the energy was fully dissipated over the course of 0.5 - 1.0 ps, and equilibrated until termination of the run. Using this approach it is possible to migrate from minima to minima which is essential when dealing with a large number of water molecules in the clusters due to a shallow potential energy surface. After a terminated simulated annealing run, several snapshots of the structures are further geometry optimized using the M06-2X/6-311++G(3df,3pd) level of theory to yield the final structures, and the identified lowest energy conformation for each morphology is then subsequently used to calculate the optical properties. The purpose of our sampling procedure is thus not to locate the global minimum, which would be very time consuming when including large clusters and would involve countless local minima conformations. The applied methodology allows us to find a local (and perhaps a good guess for the global) minimum corresponding to each cluster morphology.

Structures with more than 10 water molecules are handled differently. The clusters are only sampled in intervals of 5 water up to a maximum of 50 water molecules. The clusters are minimized with a molecular mechanics force field (UFF) using a steepest descent algorithm while attempting to keep the cluster as spherical as possible in order to represent a forming droplet. This approach does not yield accurate structures since the molecular mechanics force field is unable to handle bond breaking, but is a good compromise for investigating larger clusters without using expensive Born Oppenheimer molecular dynamics or extensive sampling.

3.2 - Optical Properties

To find a suitable methodology for calculating the optical properties of pre-nucleation clusters, a DFT functional and basis set analysis was performed for the smallest cluster subunits H_2SO_4 , NH_3 and H_2O . The performance of calculating the mean isotropic polarizability was tested using CC2, CCSD, CCSD(T), CAM-B3LYP, B3LYP, M06-2X and PW91 using various correlation consistent basis sets. On the basis of this analysis, we find that CAM-B3LYP/aug-cc-pVDZ is a good compromise between efficiency and accuracy yielding good agreement with both experimental and CCSD(T) values of the polarizability. The complete basis set and functional analysis is available in the supplementary information. Furthermore the CAM-B3LYP functional has been successfully employed in the calculation of various response properties such as polarizabilities^{70,71}, absorption properties⁷², van

der Waals C_6 -coefficients⁷⁰, natural-⁷³ and magnetic circular dichroism^{74,75}. Very recently CAM-B3LYP showed an adequate performance in calculating the hyper Rayleigh scattering of large chromophores⁷⁶. All presented calculated properties are given in atomic units (a.u.).

4 - Results and Discussion

4.1 - Cluster Structures and Relative Stabilities

The structure of the identified pre-nucleation molecular clusters are all given in the supporting information. The sampled morphologies yield very varying relative Gibb's free energies, which implies that a single morphology most likely dominates within each cluster. In Figure 2, the identified lowest Gibb's free energy molecular clusters are shown for each morphology of the $(\text{H}_2\text{SO}_4)(\text{H}_2\text{O})_n$ clusters with $n=2-10$. It is generally seen that the water molecules are distributed evenly in order to participate in more hydrogen binding sites to the polar sulfuric acid molecule. When there are 4 or more water molecules at a single site in the sampled cluster conformations, sulfuric acid is found to partially (clusters with 3,4,6 and 9 water) or fully (clusters 5,7,8,10) dissociate its proton.

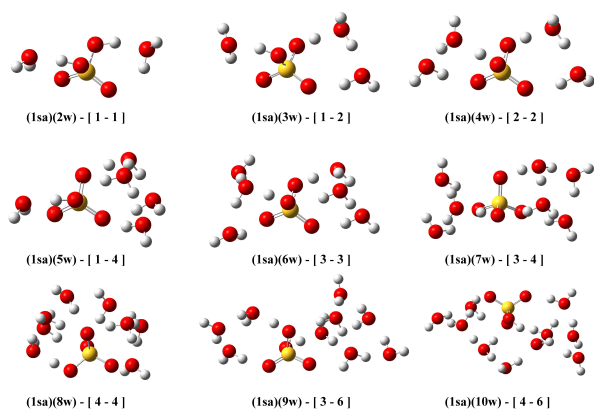


Fig. 2 The identified lowest Gibb's free energy structures of $(\text{H}_2\text{SO}_4)(\text{H}_2\text{O})_n$ clusters with n between 2 and 10.

It is seen that the lowest identified structures yield a bridging between the different sites in the case of the $(\text{H}_2\text{SO}_4)(\text{H}_2\text{O})_8$ and $(\text{H}_2\text{SO}_4)(\text{H}_2\text{O})_{10}$ clusters resulting in more spherical morphologies.

In Figure 3, the identified lowest Gibb's free energy molecular clusters are shown for each morphology in the case of the $(\text{H}_2\text{SO}_4)(\text{NH}_3)(\text{H}_2\text{O})_n$ clusters with $n=2-10$. Similarly to the $(\text{H}_2\text{SO}_4)(\text{H}_2\text{O})_n$ clusters, the water molecules are observed to locate relatively evenly around the sulfuric acid molecule. When ammonia is present at a site with two or more water

molecules, a proton transfer is observed as seen in Figure 3, forming the ammonium ion, which indicates that there is more direct ionic structure in the $(\text{H}_2\text{SO}_4)(\text{NH}_3)(\text{H}_2\text{O})_n$ clusters compared to the clusters without ammonia where in most cases only a partial proton transfer is found.

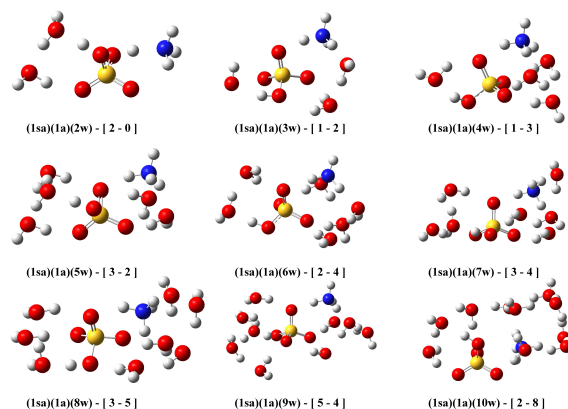


Fig. 3 The identified lowest Gibb's free energy structures of $(\text{H}_2\text{SO}_4)(\text{NH}_3)(\text{H}_2\text{O})_n$ clusters with n between 2 and 10.

The larger clusters were handled using a molecular mechanics approach and the structure of the largest investigated $(\text{H}_2\text{SO}_4)(\text{H}_2\text{O})_{50}$ and $(\text{H}_2\text{SO}_4)(\text{NH}_3)(\text{H}_2\text{O})_{50}$ clusters obtained from the simulated annealing calculation can be seen in Figure 4.

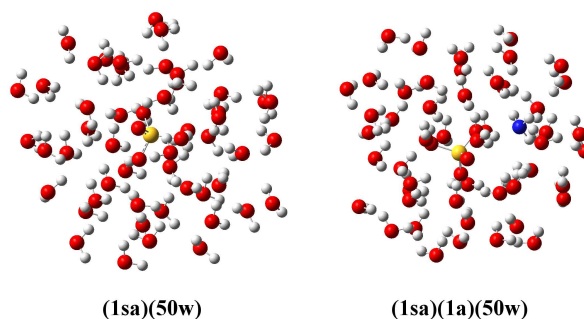


Fig. 4 Molecular structure of the largest investigated clusters: The $(\text{H}_2\text{SO}_4)(\text{H}_2\text{O})_{50}$ cluster (*Left*) and the $(\text{H}_2\text{SO}_4)(\text{NH}_3)(\text{H}_2\text{O})_{50}$ cluster (*Right*)

4.2 - Rayleigh Light Scattering Activities

4.2.1 - $(\text{H}_2\text{SO}_4)(\text{H}_2\text{O})_n$ Clusters

Using the above identified molecular structures, it is possible to calculate the Boltzmann weighted (298K) static scattering properties of the clusters. A complete list of all the individual scattering intensities for each cluster conformation is given in the supporting information. It is observed that all the different conformations within each cluster yield very similar (within 2 a.u.) isotropic mean polarizabilities $\bar{\alpha}$. For the small clusters with up to 10 water molecules the $\bar{\alpha}$ -values are found to be close to additively dependent on the cluster constituents, with only a slight cluster binding isotropic mean polarizability of at the most $\sim 3\%$. This is consistent with the study of $(\text{H}_2\text{O})_n$ clusters by Ghanty and Ghosh, who found a near additive dependence of the polarizability on the number of water molecules⁷⁷.

The larger clusters yield significantly higher binding polarizabilities of up to 240 a.u. corresponding to $\sim 10\%$ in the case of the largest $(\text{H}_2\text{SO}_4)(\text{H}_2\text{O})_{50}$ cluster. This is due to the larger hydrogen bonding network as the water content increases. The anisotropic polarizability $\Delta\alpha$ is contrarily found to be very dependent on the different conformations within each cluster and vary up to 12 a.u.. This corresponds to a binding anisotropic polarizability increase of up to 65% for the clusters with up to 10 water molecules. The highest anisotropic polarizabilities are found for clusters where the water is evenly residing around the sulfuric acid molecule. For the larger systems, where the clusters attain a spherical shape, the binding anisotropy decrease drastically between 13-24 a.u., corresponding to a drop of up to 293%. This implies that the Rayleigh scattering intensities will be very dependent on the morphology and water content of the cluster. In Figure 5, the Rayleigh light scattering intensity of natural light \mathfrak{R}_n and the depolarization ratios ρ_n of the $(\text{H}_2\text{SO}_4)(\text{H}_2\text{O})_n$ clusters can be seen as a function of the number of water molecules in the cluster.

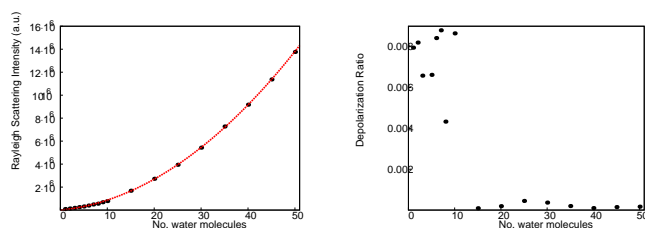


Fig. 5 Left: Rayleigh scattering intensities (\mathfrak{R}_n) from $(\text{H}_2\text{SO}_4)(\text{H}_2\text{O})_n$ clusters as a function of water molecules. The red dotted line correspond to a quadratic fit to the calculated data points (\bullet). Right: Depolarization ratio ρ_n as a function of the number of water molecules.

It is observed that the \mathfrak{R}_n scattering intensities are gradually increasing with the number of water molecules. This non-linear dependence is observed to closely follow the trend of a second order polynomial (red dotted line in Figure 5). This increasing trend can be attributed to the gradually increasing binding polarizability of the clusters, such that the $(\bar{\alpha})^2$ term in equation 4 will dominate in the Rayleigh scattering of larger particles.

The calculated depolarization ratios ρ_n are observed to rapidly decay as the cluster grows. This is due to increase in the mean isotropic polarizability with number of molecules in combination with the anisotropic polarizability being relatively constant in the range of 5-27 a.u. This is consistent with what is to be expected as the cluster change from a molecular cluster into a spherical isotropic particle. The depolarization ratios for clusters with 1-10 water molecules is seen to fluctuate from 0.004 to 0.009 and then plummet to $\sim 10^{-4}$ for the larger clusters.

The calculated scattering properties are dependent on the wavelength of the incident light. The frequency dependences on the \mathfrak{R}_n scattering intensities and ρ_n depolarization ratios were investigated for the clusters containing up to 10 water molecules in the frequency range from 200 to 800 nm. At ground level almost all incident light below 250 nm is absorbed by the atmosphere, with the highest solar intensity being in the visible range of 400-700 nm. The behaviour of all the clusters were found to depend similarly on the frequency. At 800 nm the \mathfrak{R}_n scattering intensities are found to increase 2% compared to the static limit. This gradually increases with higher frequency leading to 16-18% increase at 300nm and a 48-56% increase at 200 nm. The depolarization ratios ρ_n also show a slight dependence on the wavelength. At 800 nm only a 1-2% increase is observed. Similar to the scattering, this gradually increase with increased frequency, with a 1-13% increase at 300 nm and up to a 41% increase at 200 nm.

4.2.1 - $(\text{H}_2\text{SO}_4)(\text{NH}_3)(\text{H}_2\text{O})_n$ Clusters

For the $(\text{H}_2\text{SO}_4)(\text{NH}_3)(\text{H}_2\text{O})_n$ with $n \leq 10$ clusters, it is observed that the different conformations within each cluster morphology yield isotropic mean binding polarizabilities $\bar{\alpha}$ within 2 a.u. corresponding to up to 2% increase. For the larger clusters with n up to 50 the binding polarizability reaches up to 65 a.u. corresponding to a maximum of 14%. The binding anisotropic polarizabilities are found to vary up to 16 a.u. in the clusters with 1-10 water molecules, corresponding to up to a 68% increase. In the larger clusters, the binding anisotropies are found to decrease up to 30 a.u. which corresponds up to a 444% decrease in binding anisotropy in the case of the $(\text{H}_2\text{SO}_4)(\text{NH}_3)(\text{H}_2\text{O})_{30}$ cluster. In Figure 6, the Rayleigh light scattering \mathfrak{R}_n and ρ_n for the $(\text{H}_2\text{SO}_4)(\text{NH}_3)(\text{H}_2\text{O})_n$ clusters are plotted as a

function of the number of water molecules in the cluster. The scattering intensities for these clusters are similar to the case without ammonia seen to follow a quadratic fit (red dotted line). It is observed that the scattering activities of the $(\text{H}_2\text{SO}_4)(\text{NH}_3)(\text{H}_2\text{O})_n$ clusters are larger than for the $(\text{H}_2\text{SO}_4)(\text{H}_2\text{O})_n$ clusters on a per molecule basis. This difference is partly due to the higher polarizability of an ammonia molecule compared to a water molecule with $\bar{\alpha}$ equal to 9.27 a.u. and 13.91 a.u., respectively. The main difference can however be attributed to the induced anisotropy in the cluster containing ammonia. In the case of the larger clusters the anisotropic polarizability goes from a maximum of 19.54 a.u. up to 41.91 a.u. when an ammonia molecule is present. This could indicate that complex clusters could potentially show high Rayleigh scattering intensities. The depolarization ratios for the $(\text{H}_2\text{SO}_4)(\text{NH}_3)(\text{H}_2\text{O})_n$ clusters are in the same range ($10^{-4} - 10^{-2}$) as the clusters without ammonia present.

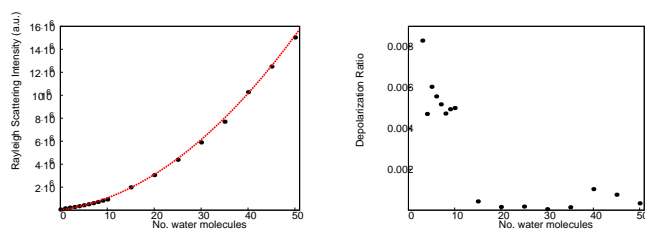


Fig. 6 *Left:* Rayleigh scattering intensities (\mathfrak{R}_n) from $(\text{H}_2\text{SO}_4)(\text{NH}_3)(\text{H}_2\text{O})_n$ clusters as a function of the number of water molecules. The red dotted line represents a quadratic fit to the calculated data points (\bullet). *Right:* Depolarization ratio ρ_n as a function of the number of water molecules.

The frequency dependence was also investigated for a subset of the $(\text{H}_2\text{SO}_4)(\text{NH}_3)(\text{H}_2\text{O})_n$ clusters with up to 10 water molecules. The $(\text{H}_2\text{SO}_4)(\text{NH}_3)(\text{H}_2\text{O})_n$ clusters show a similar dependence on the frequency as the $(\text{H}_2\text{SO}_4)(\text{H}_2\text{O})_n$ clusters. At 800 nm the \mathfrak{R}_n scattering intensities are, in all cases, observed to increase 2% compared to the static limit. This gradually increases with the frequency, leading to 18-19% increase at 300 nm and a 56-64% increase at 200 nm. The depolarization ratios ρ_n also show a similar dependence on the wavelength. At 800 nm only a 2% increase is observed which gradually increase with increased frequency, with a 3-22% increase at 300 nm and up to a 94% increase at 200 nm. Thereby, it is seen that the wavelength dependence for the $(\text{H}_2\text{SO}_4)(\text{NH}_3)(\text{H}_2\text{O})_n$ clusters is slightly higher than for the $(\text{H}_2\text{SO}_4)(\text{H}_2\text{O})_n$ clusters.

4.3 - Hyper-Rayleigh Light Scattering Activities

4.3.1 - $(\text{H}_2\text{SO}_4)(\text{H}_2\text{O})_n$ Clusters

The Boltzmann weighted (298 K) static hyper Rayleigh scattering activities ($\mathfrak{R}_{\text{HRS}}$) have been calculated for the same

clusters as above. A complete list of the scattering activities for each cluster conformation is given in the supporting information. It is observed that the different conformations within each cluster yield varying hyper Rayleigh scattering values. This indicates that the $\mathfrak{R}_{\text{HRS}}$ -value is very dependent on the cluster morphology. In Figure 7, the calculated hyper Rayleigh scattering activities of the $(\text{H}_2\text{SO}_4)(\text{H}_2\text{O})_n$ clusters can be seen as a function of water molecules.

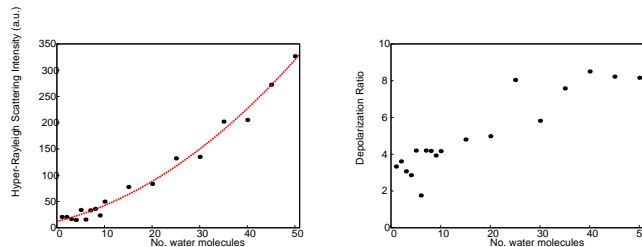


Fig. 7 *Left:* Hyper Rayleigh scattering intensities ($\mathfrak{R}_{\text{HRS}}$) from $(\text{H}_2\text{SO}_4)(\text{H}_2\text{O})_n$ clusters as a function of water molecules. The red dotted line corresponds to a quadratic fit to the calculated data points (\bullet). *Right:* Hyper depolarization ratio ρ_{HRS} as a function of water molecules.

For the clusters containing 10 water molecules or less, the $\mathfrak{R}_{\text{HRS}}$ -value varies between 15-50 a.u.. The hyper Rayleigh scattering activity is observed to grow with increasing water content similarly to what is observed for the ordinary Rayleigh scattering. Due to the sensitivity of the $\mathfrak{R}_{\text{HRS}}$ -value to the molecular structure, it is difficult to determine whether the growth is linear or quadratic. In Figure 7 the red dotted line correspond to a quadratic fit to the calculated data points. The depolarization ratio is seen to increase from a value ~ 3 -4 to ~ 8 with higher water content. Thereby, as the cluster grows, it changes from partial octopolar character to purely dipolar character as the water content gets around 35-50 water molecules.

4.3.2 - $(\text{H}_2\text{SO}_4)(\text{NH}_3)(\text{H}_2\text{O})_n$ Clusters

The Boltzmann weighted (298 K) static hyper Rayleigh scattering activities ($\mathfrak{R}_{\text{HRS}}$) have similarly been calculated for the $(\text{H}_2\text{SO}_4)(\text{NH}_3)(\text{H}_2\text{O})_n$ with n up to 40. A complete list of the scattering activities for each cluster conformation is given in the supporting information. Similarly to the $(\text{H}_2\text{SO}_4)(\text{H}_2\text{O})_n$ clusters, the different cluster morphologies yield varying hyper Rayleigh scattering values. In Figure 8, the calculated hyper Rayleigh scattering activities of the $(\text{H}_2\text{SO}_4)(\text{NH}_3)(\text{H}_2\text{O})_n$ clusters can be seen as a function of the number of water molecules.

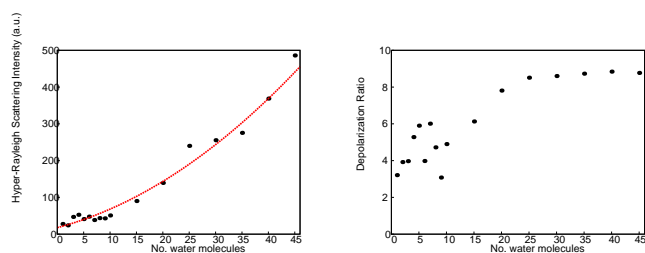


Fig. 8 *Left*: Hyper Rayleigh scattering intensities (\mathfrak{R}_{HRS}) from $(\text{H}_2\text{SO}_4)(\text{NH}_3)(\text{H}_2\text{O})_n$ clusters as a function of water molecules. The red dotted line correspond to a quadratic fit to the calculated data points (\bullet). *Right*: Hyper depolarization ratio ρ_{HRS} as a function of water molecules.

The different cluster conformations were found to show hyper Rayleigh scattering activities that vary up to 30 a.u. within each cluster type. Similarly to the $(\text{H}_2\text{SO}_4)(\text{H}_2\text{O})_n$ clusters, the scattering is observed to grow as a function of the water content. The red dotted line in Figure 8 correspond to a quadratic fit to the data points. The $(\text{H}_2\text{SO}_4)(\text{NH}_3)(\text{H}_2\text{O})_n$ clusters with n up to 10 generally show slightly higher hyper depolarization ratios in the range 3 to 6 than the $(\text{H}_2\text{SO}_4)(\text{H}_2\text{O})_n$ clusters with values around 2 to 4. Similarly to the $(\text{H}_2\text{SO}_4)(\text{H}_2\text{O})_n$ clusters the hyper depolarization ratio changes from a slight octopolar character for the small clusters to purely asymmetrically dipolar for the clusters with more than 25 water molecules.

5 - Conclusion

We have investigated the scattering properties of atmospheric pre-nucleation clusters using a quantum mechanical response theory framework. As model systems we have investigated the $(\text{H}_2\text{SO}_4)(\text{H}_2\text{O})_n$ and $(\text{H}_2\text{SO}_4)(\text{NH}_3)(\text{H}_2\text{O})_n$ clusters. While these clusters are most likely short-lived in the atmosphere and prone to rapid evaporation our study serves as the first scattering investigation of relevance to the Earth's atmosphere of pre-nucleation clusters from a bottom up approach using classical Rayleigh scattering theory.

We find that the linear Rayleigh scattering activity depends quadratically on the water content. It is dependent on the cluster constituents where a single ammonia molecule is able to induce a high anisotropy in the particle, which on a per molecule basis yield an increased scattering. The hyper Rayleigh scattering activities are in all cases found to be relatively low and hence the frequency doubled hyper Rayleigh scattering is negligible from these particles.

We have made an elaborate study of the structural dependence of the molecular cluster morphologies on the scattering properties. Since the ordinary Rayleigh scattering is found to only depend slightly on cluster morphology, identified mini-

mum cluster structures will dominate the scattering properties. From our investigation it is clear that in order to get insight into the Rayleigh scattering properties of a given molecular cluster it is possible to perform a CAM-B3LYP/aug-cc-pvdz calculation on top of an identified lowest energy cluster.

As a single ammonia molecule is able to induce a high anisotropy in relatively isotropic particles, it could indicate that clusters consisting of complex mixtures of compounds could show high scattering activities. This could be particularly relevant for pre-nucleation clusters containing a mixture of organics, sulfuric acid, ammonia and water.

Acknowledgement

The authors thank the Danish Center for Scientific Computing for providing computer resources, the Danish Natural Science Research Council/The Danish Councils for Independent Research. The Villum Kann Rasmussen Foundation for and the Nordic Center of Excellence (CRAICC) financial support. Jonas Elm thank the CoDECS network for financial support of this project.

References

- 1 U. Lohmann and J. Feichter, *Atmos. Phys. Chem.*, 2005, **5**, 715–737.
- 2 J. Haywood and O. Boucher, *Rev. Geophys.*, 2000, **38**, 513–543.
- 3 U. Poschl, *Angew. Chem. Int. Ed.*, 2005, **44**, 7520–7540.
- 4 M. Kulmala, J. Kontkanen, H. Junninen, K. Lehtipalo, H. E. Manninen, T. Nieminen, T. Petj, M. Sipil, S. Schobesberger, P. Rantala, A. Franchin, T. Jokinen, E. Jrvinen, M. Ijl, J. Kangasluoma, J. Hakala, P. P. Aalto, P. Paasonen, J. Mikkil, J. Vanhanen, J. Aalto, H. Hakola, U. Makkonen, T. Ruuskanen, R. L. Mauldin, J. Duplissy, H. Vehkamäki, J. Bck, A. Kotrelainen, I. Riipinen, T. Kurtin, M. V. Johnston, J. N. Smith, M. Ehn, T. F. Mentel, K. E. J. Lehtinen, A. Laaksonen, V.-M. Kerminen and D. R. Worsnop, *Science*, 2013, **339**, 943–946.
- 5 T. Kurtén, M. R. Sundberg, H. Vehkamäki, M. Noppel, J. Blomqvist and M. Kulmala, *J. Phys. Chem. A*, 2006, **110**, 7178–7188.
- 6 T. Kurtén, L. Torpo, M. R. Sundberg, V. Kerminen, H. Vehkamäki and M. Kulmala, *Atmos. Chem. Phys.*, 2007, **7**, 2765–2773.
- 7 T. Kurtén, L. Torpo, C. Ding, H. Vehkamäki, M. R. Sundberg, K. Laasonen and M. Kulmala, *J. Geophys. Res.*, 2007, **112**, D04210.
- 8 L. Torpo, T. Kurtén, H. Vehkamäki, K. Laasonen, M. R. Sundberg and M. Kulmala, *J. Phys. Chem. A*, 2007, **111**, 10671–10674.
- 9 J. Herb, A. B. Nadykto and F. Yu, *Chem. Phys. Lett.*, 2011, **518**, 7–14.
- 10 T. Kurtén, V. Loukonen, H. Vehkamäki and M. Kulmala, *Atmos. Chem. Phys.*, 2008, **8**, 4095–4103.
- 11 V. Loukonen, T. Kurtén, I. K. Ortega, H. Vehkamäki, A. A. H. Pádua, K. Sellgri and M. Kulmala, *Atmos. Chem. Phys.*, 2010, **10**, 4961–4974.
- 12 A. B. Nadykto, F. Yu, M. V. Jakovleva, J. Herb and Y. Xu, *Entropy*, 2011, **13**, 554–569.
- 13 P. Paasonen, T. Olenius, O. Kupiainen, T. Kurtén, T. Petäjä, W. Birmili, A. Hamed, M. Hu, L. G. Huey, C. Plass-Duelmer and et al, *Atmos. Chem. Phys.*, 2012, **12**, 9113–9133.
- 14 M. J. Ryding, K. Ruusuvoori, P. U. Andersson, A. S. Zatul, M. J. McGrath, T. Kurtén, I. K. Ortega, H. Vehkamäki and E. Uggerud, *J. Phys. Chem. A*, 2012, **116**, 4902–4908.
- 15 O. Kupiainen, I. K. Ortega, T. Kurtén and H. Vehkamäki, *Atmos. Chem. Phys.*, 2012, **12**, 3591–3599.

- 16 J. Almeida, S. Schobesberger, A. Kurten, I. K. Ortega, O. Kupiainen-Maatta, A. P. Praplan, A. Adamov, A. Amorim, F. Bianchi, M. Breitenlechner, A. David, J. Dommen, N. M. Donahue, A. Downard, E. Dunne, J. Duplissy, S. Ehrhart, R. C. Flagan, A. Franchin, R. Guida, J. Hakala, A. Hansel, M. Heinritzi, H. Henschel, T. Jokinen, H. Junninen, M. Kajos, J. Kangasluoma, H. Keskinen, A. Kupc, T. Kurten, A. N. Kvashin, A. Laaksonen, K. Lehtipalo, M. Leiminger, J. Leppa, V. Loukonen, V. Makhmutov, S. Mathot, M. J. McGrath, T. Nieminen, T. Olenius, A. Onnela, T. Petaja, F. Riccobono, I. Riipinen, M. Rissanen, L. Rondo, T. Ruuskanen, F. D. Santos, N. Sarnela, S. Schallhart, R. Schnitzhofer, J. H. Seinfeld, M. Simon, M. Sipila, Y. Stozhkov, F. Stratmann, A. Tome, J. Trostl, G. Tsagkogeorgas, P. Vaattovaara, Y. Viisanen, A. Virtanen, A. Vrtala, P. E. Wagner, E. Weingartner, H. Wex, C. Williamson, D. Wimmer, P. Ye, T. Yli-Juuti, K. S. Carslaw, M. Kulmala, J. Curtius, U. Baltensperger, D. R. Worsnop, H. Vehkamäki and J. Kirkby, *Nature*, 2013, **502**, 359–363.
- 17 A. B. Nadykto and F. Yu, *Chem. Phys. Lett.*, 2007, **435**, 14–18.
- 18 C. D. O'Dowd, P. Aalto, K. Hmeri, M. Kulmala and T. Hoffmann, *Nature*, 2002, **416**, 497–498.
- 19 R. Zhang, I. Suh, J. Zhao, D. Zhang, E. C. Fortner, X. Tie, L. T. Molina and M. J. Molina, *Science*, 2004, **304**, 1487–1490.
- 20 J. Elm, M. Bilde and K. V. Mikkelsen, *J. Phys. Chem. A*, 2013, **113**, 6695–6701.
- 21 M. Sloth, M. Bilde and K. V. Mikkelsen, *Mol. Phys.*, 2005, **102**, 2361–2368.
- 22 H. Falsig, A. Gross, J. Kongsted, A. Osted, M. Sloth, K. V. Mikkelsen and O. Christiansen, *J. Phys. Chem. A*, 2006, **110**, 660–670.
- 23 Y. Xu, A. B. Nadykto, F. Yu, L. Jiang and W. Wang, *J. mol. Struct.-THEOCHEM*, 2010, **951**, 28–33.
- 24 Y. Xu, A. B. Nadykto, F. Yu, J. Herb and W. Wang, *J. Phys. Chem. A*, 2010, **114**, 387–396.
- 25 L. Wang, A. F. Khalizov, J. Zheng, W. Xu, Y. Ma, V. Lal, and R. Zhang, *NATURE GEOSCIENCE*, 2010, **3**, 238–242.
- 26 W. Xu and R. Zhang, *J. Phys. Chem. A*, 2012, **116**, 4539–4550.
- 27 K. H. Weber, F. J. Morales and F. Tao, *J. Phys. Chem. A*, 2012, **116**, 11601–11617.
- 28 R. Zhang, *Science*, 2010, **328**, 1366–1367.
- 29 R. Zhang, L. Wang, A. F. Khalizov, J. Zhao, J. Zheng, R. L. McGraw and L. T. Molina, *PNAS*, 2009, **106**, 17650–17654.
- 30 J. Zhao, A. Khalizov, R. Zhang and R. L. McGraw, *J. Phys. Chem. A*, 2009, **113**, 680–689.
- 31 W. Xu and R. Zhang, *J. Chem. Phys.*, 2013, **139**, 064312:1–11.
- 32 S. Schobesberger, H. Junninen, F. Bianchi, G. Lönn, M. Ehn, K. Lehtipalo, J. Dommen, S. Ehrhart, I. K. Ortega, A. Franchin, T. Nieminen, F. Riccobono, M. Hutterli, J. Duplissy, J. Almeida, A. Amorim, M. Breitenlechner, A. J. Downard, E. M. Dunne, R. C. Flagan, M. Kajos, H. Keskinen, J. Kirkby, A. Kupc, A. Kürten, T. Kurtén, A. Laaksonen, S. Mathot, A. Onnela, A. P. Praplan, L. Rondo, F. D. Santos, S. Schallhart, R. Schnitzhofer, M. Sipilä, A. Tomé, G. Tsagkogeorgas, H. Vehkamäki, D. Wimmer, U. Baltensperger, K. S. Carslaw, J. Curtius, A. Hansel, T. Petäjä, M. Kulmala, N. M. Donahue and D. R. Worsnop, *PNAS*, 2013, **110**, 17223–17228.
- 33 A. Metzger, B. Verheggen, J. Dommen, J. Duplissy, A. S. H. Prevot, E. Weingartner, I. Riipinen, M. Kulmala, D. V. Spracklen, K. S. Carslaw and U. Baltensperger, *PNAS*, 2010, **107**, 6646–6651.
- 34 G.-L. Hou, W. Lin, S. H. M. Deng, J. Zhang, W.-J. Zheng, F. Paesani and X.-B. Wang, *The Journal of Physical Chemistry Letters*, 2013, **4**, 779–785.
- 35 J. Elm, M. Bilde and K. V. Mikkelsen, *J. Phys. Chem. A*, 2013, **117**, 12990–12997.
- 36 N. M. Donahue, I. K. Ortega, W. Chuang, I. Riipinen, F. Riccobono, S. Schobesberger, J. Dommen, U. Baltensperger, M. Kulmala, D. R. Worsnop and H. Vehkamäki.
- 37 I. Riipinen, T. Yli-Juuti, J. R. Pierce, T. Petäjä, D. R. Worsnop, M. Kulmala and N. M. Donahue, *Nature Geoscience*, 2012, **5**, 453–458.
- 38 T. Kurtén, M. Noppel, H. Vehkamäki, M. Salonen and M. Kulmala, *Boreal Env. Res.*, 2007, **12**, 431–453.
- 39 I. K. Ortega, T. Kurtén, H. Vehkamäki and M. Kulmala, *Atmos. Chem. Phys.*, 2008, **8**, 2859–2867.
- 40 A. B. Nadykto, F. Yu and J. Herb, *Int. J. Mol. Sci.*, 2008, **9**, 2184–2193.
- 41 A. B. Nadykto, F. Yu and J. Herb, *Atmos. Chem. Phys.*, 2009, **9**, 4031–4039.
- 42 A. B. Nadykto, F. Yu and J. Herb, *Chem. Phys.*, 2009, **360**, 67–73.
- 43 P. Hvelplund, T. Kurtén, K. Stöckel, M. J. Ryding, S. B. Nielsen and E. Uggerud, *J. Phys. Chem. A*, 2010, **114**, 7301–7310.
- 44 N. Bork, T. Kurtén, M. B. Enghoff, J. O. P. Pedersen, K. V. Mikkelsen and H. Svensmark, *Atmos. Chem. Phys.*, 2011, **11**, 7133–7142.
- 45 N. Bork, T. Kurtén, M. B. Enghoff, J. O. P. Pedersen, K. V. Mikkelsen and H. Svensmark, *Atmos. Chem. Phys.*, 2012, **12**, 3639–3652.
- 46 D. E. Husar, B. Temelso, A. L. Ashworth and G. C. Shields, *J. Phys. Chem. A*, 2012, **116**, 5151–5163.
- 47 G. Mie, *Annalen der Physik*, 1908, **330**, 377–445.
- 48 J. Strutt, *Philos. Mag.*, 1871, **41**, 107–120, 274–279.
- 49 J. Strutt, *Philos. Mag.*, 1871, **41**, 447–454.
- 50 J. Strutt, *Philos. Mag.*, 1881, **12**, 81–101.
- 51 J. Strutt, *Philos. Mag.*, 1899, **47**, 375–394.
- 52 M. Kulmala, I. Riipinen, M. Sipilä, H. E. Manninen, T. Petäjä, H. Junninen, M. Dal Maso, G. Mordas, A. Mirme, M. Vana, A. Hirsikko, L. Laakso, R. M. Harrison, I. Hanson, C. Leung, K. E. J. Lehtinen and V. Kerminen, *Science*, 2007, **318**, 89–92.
- 53 M. Sipilä, K. Lehtipalo, M. Kulmala, T. Petäjä, H. Junninen, P. P. Aalto, H. E. Manninen, E. Kyrö, E. Asmi, I. Riipinen, J. Curtius, A. Kurten, S. Borrmann and C. D. O'Dowd, *Atmos. Chem. Phys.*, 2008, **8**, 4049–4060.
- 54 K. Lehtipalo, M. Sipilä, I. Riipinen, T. Nieminen and M. Kulmala, *Atmos. Chem. Phys.*, 2009, **9**, 4177–4184.
- 55 H. E. Manninen, T. Petaja, E. Asmi, I. Riipinen, T. Nieminen, J. Mikkila, U. Horrak, A. Mirme, S. Mirme, L. Laakso, V. M. Kerminen and M. Kulmala, *Boreal Env. Res.*, 2009, **14**, 591–605.
- 56 A. M. Bush, A. J. Bell, J. G. Frey and J. M. Mestdagh, *J. Phys. Chem. A*, 1998, **102**, 6457–6463.
- 57 E. Rissi, E. E. Fileti and S. Canuto, *Theor. Chem. Acc.*, 2003, **110**, 360–366.
- 58 E. E. Fileti, R. Rivelino and S. Canuto, *J. Phys. B: At. Mol. Opt. Phys.*, 2003, **36**, 399–408.
- 59 P. Chaudhuri and S. Canuto, *J. Mol. Struct.: THEOCHEM*, 2006, **760**, 15–20.
- 60 E. Orestes, P. Chaudhuri and S. Canuto, *Mol. Phys.*, 2012, **110**, 297–306.
- 61 A. M. da Silva, S. Chakraborty and P. Chaudhuri, *Int. J. Quant. Chem.*, 2012, **112**, 2822–2827.
- 62 A. Plaquet, M. Guillaume, B. Champagne, F. Castet, L. Ducasse, J. L. Pozzo and V. Rodriguez, *Phys. Chem. Chem. Phys.*, 2008, **10**, 6223–6232.
- 63 J. Olsen and P. Jørgensen, *J. Chem. Phys.*, 1985, **82**, 3235–3264.
- 64 *Gaussian 09, Revision B.01*, M. J. Frisch, G. W. Trucks, H. B. Schlegel, G. E. Scuseria, M. A. Robb, J. R. Cheeseman, G. Scalmani, V. Barone, B. Mennucci, G. A. Petersson, et al., *Gaussian, Inc., Wallingford CT, 2010*.
- 65 J. Elm, M. Bilde and K. V. Mikkelsen, *J. Chem. Theory Comput.*, 2012, **8**, 2071–2077.
- 66 J. Elm, M. Bilde and K. V. Mikkelsen, *Phys. Chem. Chem. Phys.*, 2013, **15**, 16442–16445.
- 67 H. R. Leverentz, J. I. Siepmann, D. G. Truhlar, V. Loukonen and H. Vehkamäki, *J. Phys. Chem. A*, 2013, **117**, 3819–3825.
- 68 N. Bork, L. Du and H. G. Kjaergaard, *J. Phys. Chem. A*, 2014, **118**, 1384–1389.
- 69 Y. Zhao and D. G. Truhlar, *Theor. Chem. Account.*, 2008, **120**, 215–241.

-
- 70 J. Kauczor, P. Norman and W. A. Saidi, *J. Chem. Phys.*, 2013, **138**, doi: 10.1063/1.4795158.
- 71 P. A. Limacher, K. V. Mikkelsen and H. P. Lüthi, *J. Chem. Phys.*, 2009, **130**, doi: 10.1063/1.3139023.
- 72 P. Lind, M. Carlsson, B. Eliasson, E. Glimsdal, M. Lindgren, C. Lopes, L. Boman and P. Norman, *Mol. Phys.*, 2009, **107**, 629–641.
- 73 A. Jiemchoorj and P. Norman, *J. Chem. Phys.*, 2008, **128**, doi: 10.1063/1.2937906.
- 74 H. Solheim, K. Ruud, S. Coriani and P. Norman, *J. Chem. Phys.*, 2008, **128**, doi: 10.1063/1.2834924.
- 75 T. Fahleson, J. Kauczor, P. Norman and S. Coriani, *Mol. Phys.*, 2013, **111**, 1401–1404.
- 76 B. F. Milne, P. Norman, F. Nogueira and C. Cardoso, *Phys. Chem. Chem. Phys.*, 2013, **15**, 14814–14822.
- 77 T. K. Ghanty and S. K. Ghosh, *J. Chem. Phys.*, 2003, **118**, 8547–8550.

Table of Contents Entry

Table of contents entry:

The Rayleigh light scattering properties of pre-nucleation molecular clusters are assessed using density functional theory.

Graphic

